# Swift-uranium-ion-induced damage in sapphire

B. Canut

*Département de Physique des Matériaux (URA CNRS 172), CNRS et Université Claude Bernard-Lyon I,*
*69622 Villeurbanne Cédex, France*


A. Benyagoub and G. Marest

*Institut de Physique Nucléaire de Lyon (IN₂P₃), CNRS et Université Claude Bernard-Lyon I, 69622 Villeurbanne, Cédex, France*


A. Meftah

*Centre Interdisciplinaire de Recherches avec les Ions Lourds, Ganil, boulevard Antoine Becquerel, 14040 Caen Cédex, France*


N. Moncoffre

*Institut de Physique Nucléaire de Lyon (IN₂P₃), CNRS et Université Claude Bernard-Lyon I, 69622 Villeurbanne Cédex, France*


S. M. M. Ramos

*Département de Physique des Matériaux (URA CNRS 172), CNRS et Université Claude Bernard-Lyon I,*
*69622 Villeurbanne Cédex, France*


F. Studer

*Laboratoire de Cristallographie et Sciences des Matériaux, Institut des Sciences de la Matière et du Rayonnement,*
*boulevard du Maréchal Juin 14032 Caen Cédex, France*


P. Thevenard

*Département de Physique des Matériaux (URA CNRS 172), CNRS et Université Claude Bernard-Lyon I,*
*69622 Villeurbanne Cédex, France*


M. Toulemonde

*Centre Interdisciplinaire de Recherches avec les Ions Lourds, Ganil, boulevard Antoine Becquerel, 14040 Caen Cédex, France*

Single crystals of $\alpha$-Al$_2$O$_3$ were irradiated at Ganil with $^{238}$U ions using four different energies: 0.48, 1.72, 2.78, and 3.40 MeV/u. All the irradiations were performed at a temperature of $\approx 80$ K, with fluences extending from $1.2 \times 10^{12}$ to $2.5 \times 10^{12}$ ions cm$^{-2}$. The samples were characterized by Rutherford backscattering spectrometry in channeling geometry (RBS-C) and optical absorption measurements. RBS-C analyses evidence the lattice disorder induced by collective electronic excitations. Depending on the electronic stopping power $(dE/dx)e$ (up to 44.2 keV nm$^{-1}$), the damage cross section $A_e$ varies between 0.3 and $2.1 \times 10^{-13}$ cm$^2$. Optical absorption spectroscopy exhibited the characteristic bands associated with oxygen vacancies. The kinetics of $F$ centers were determined in order to precisely determine the respective contributions of the nuclear and electronic processes in point-defect generation.

## I. INTRODUCTION

Aluminium oxide Al$_2$O$_3$ presents favorable physicochemical properties for many industrial applications: hardness, chemical insensitivity, refractory behavior ($T_m = 2318$ K), and transparency over a wide wavelength range ($\sim 0.2$–$6.0$ $\mu$m). It has been proved for many years that ion beam processing may be successfully undertaken for altering the near-surface properties of ceramics like Al$_2$O$_3$. For example, the earliest works on ion implantation in Al$_2$O$_3$ dealt with modifications in the optical properties of this material.[1-3] Then many investigations have been reported on the microstructural changes induced by ion implantation and post annealing treatments.[4-9] The effects of ion implantation on the

mechanical and tribological properties of both sapphire and polycrystalline alumina have also been studied extensively during the last two decades.[10-15] The optical, electrical, or mechanical modifications observed in irradiated ceramics like Al$_2$O$_3$ result from complex interactions involving the slowing-down process of the incident ions which induce defect creation, structural transformations, and chemical effects in the host matrix.[16] Low-dose light-ion implantations or electron irradiations of sapphire induce predominantly isolated defects, responsible for an increase of the optical absorption in the near ultraviolet wavelength range. The main absorption bands, located at 258 and 206 nm, have been identified as due to an oxygen vacancy with two trapped electrons ($F$ center) and with one trapped electron ($F^+$ center) respectively.

At low energy the damage process is associated with direct momentum transfer from the incident ions to host atoms. In this regime, according to a Kinchin-Pease description,[17] the main parameters governing the number of displaced atoms are the nuclear stopping power $(dE/dx)_n$ (predominant slowing-down process at low energies) and the displacement energy $E_d$ of the target atomic species. The binary structure of aluminium oxide leads to unequal displacement energies for anions and cations: 75 and 16 eV, respectively, according to Parkin et al.[18] It has to be noticed that even for very high fluences ($\sim 10^{17}$ ions cm$^{-2}$), the amorphization of sapphire is generally not observed, except for low-temperature (77 K) implantations.[12,19,20] However, in some cases, chemical effects of reactive implanted ions [Sn,[21] Zr,[22] and Nb (Ref. 23)] may promote the amorphization of sapphire at room temperature.

The influence of the nuclear stopping power onto the damage mechanisms of bombarded sapphire is now well established, but a controversy remains as regards the sensitivity of this material to electronic excitations. Generally, refractory oxides are known to be insensitive to ionizing radiations, as they can be observed nondestructively by low-energy electron microscopy. According to Clinard and Hobbs,[24] the creation of stable defects in the oxygen sublattice by inelastic process requires an available excitation energy comparable to the displacement energy. This criterion is not fulfilled for $Al_2O_3$ as its band gap (10 eV) is much lower than $E_d$ for oxygen atoms (75 eV). However, it has been observed for many years that collective excitations resulting from swift heavy-ion irradiations may create specific damage in a great variety of materials. Such an effect was evidenced for the first time in 1959 by Silk and Barnes.[25] They irradiated mica with uranium fission fragments and observed, by means of transmission electron microscopy, amorphous cylinders ("latent tracks") surrounding each particle trajectory. Later on, using chemical etching in many natural and synthetic oxides (including $Al_2O_3$), Sigrist and Balzer[26] showed the existence of a threshold in the electronic stopping power, characteristic of each material, for latent track revelation. A correlation was pointed out between the thermal diffusivity of the target and the corresponding $(dE/dx)_e$ threshold and no latent track revelation was obtained in $Al_2O_3$. Since the beginning of the 1980s, irradiation experiments in the electronic stopping power regime have been performed extensively in all kinds of materials, using the high-energy beams (GeV range) delivered by heavy-ion accelerators. So the key influence of $(dE/dx)_e$ has been unambiguously attested in many unexpected effects. For instance, anomalous ion-induced anisotropic plastic deformation in amorphous metallic materials,[27-32] amorphization[33] and latent track formation[34] in metallic alloys, and annealing of elastically created point defects in pure metals.[35,36]

Moreover, $(dE/dx)_e$-induced damage has been evidenced in many nonradiolysable insulators like spinels $AFe_2O_4$ (Ref. 37) (with $A=$ Ni, Mg, Zn, and Fe), yttrium iron garnet $Y_3Fe_5O_{12}$ (Ref. 38) and other magnetic insulators like $BaFe_{12}O_{19}$ (Ref. 39) and $SrFe_{12}O_{19}$.[40] Recently,

Canut et al.[41] reported on high-energy (3.5 MeV/u) Pb ion-irradiation effects in $\alpha$-$Al_2O_3$. In this preliminary work it was shown that sapphire is sensitive to high electronic energy losses, via a damage cross section of about $10^{-13}$ cm$^2$.

The aim of this paper is to confirm such a result by $^{238}$U irradiations in the GeV range. The influence of $(dE/dx)_e$ on both point and extended defect creation will be discussed.

## II. EXPERIMENTAL PROCEDURE

$\alpha$-$Al_2O_3$ single crystals of (0001) orientation with optical polished surfaces were used. Prior to the irradiations the samples were annealed in air at 1723 K for 120 h in order to remove the residual polishing surface damage. The irradiations were performed at Ganil with $^{238}$U ions of 3.40 MeV/u incident energy at equilibrium charge state, corresponding to an electronic stopping power of 44.2 keV nm$^{-1}$. The fluences ranged from $1.2\times10^{12}$ to $2.5\times10^{12}$ ions cm$^{-2}$ and the flux was about $10^8$ ions cm$^{-2}$ s$^{-1}$ on a 4.4-cm$^2$ irradiated surface. In these experiments all the crystals were maintained at liquid-nitrogen temperature ($\sim 80$ K). In order to modify the energy and consequently the electronic stopping power of the impinging beam, some samples were covered with aluminium foils of either 5, 15, or 30 $\mu$m thicknesses. The resulting initial energies and $(dE/dx)_e$ values at the surface were calculated with the TRIM91 code[42] and listed in Table I, in conjunction with the relative velocities $\beta=v/c$ (where $v$ is the velocity of the ions and $c$ is the light velocity), the projected ranges $R_p$ and the initial nuclear stopping powers $(dE/dx)_n$. It is clearly seen that, whatever the irradiation conditions, the slowing down of the uranium ions is mainly governed by electronic processes up to a depth of a few $\mu$m $[(dE/dx)_e/(dE/dx)_n\approx10^3]$. Moreover, in order to check the possible contribution of elastic processes to the damage created near the sample surface, the initial yields of displacements $Y_n$ have been also listed in Table I. These $Y_n$ values are based on the Kinchin-Pease model used in TRIM calculations, assuming displacement energies of 75 and 16 eV for oxygen and aluminium atoms, respectively. Rutherford backscattering spectrometry in

TABLE I. Main characteristics of the $^{238}$U irradiations in sapphire: absorber thickness ($t$), incident energy ($E$), relative velocity ($\beta=v/c$), projected range ($R_p$), incident electronic $[(dE/dx)_e]$ and nuclear $[(dE/dx)_n]$ stopping powers. In the last column, $Y_n$ is the theoretical yield of displacements at the sample surface calculated from TRIM91 code.

| $t$ ($\mu$m) | $E$ (MeV) | $\beta$ (%) | $R_p$ ($\mu$m) | $\left[\dfrac{dE}{dx}\right]_e$ keV nm$^{-1}$ | $\left[\dfrac{dE}{dx}\right]_n$ keV nm$^{-1}$ | $Y_n$ ($\mu$m$^{-1}$) |
|---|---|---|---|---|---|---|
| 0 | 809 | 8.54 | 26.2 | 44.2 | 0.0119 | 540 |
| 5 | 662 | 7.72 | 22.8 | 42.7 | 0.0139 | 620 |
| 15 | 410 | 6.08 | 16.7 | 38.8 | 0.0207 | 960 |
| 30 | 115 | 3.22 | 7.8 | 24.0 | 0.0567 | 2550 |

B. CANUT *et al.*

channeling geometry (RBS-C) was carried out using a $^4\text{He}^+$ beam generated by a Van de Graaff accelerator working at a maximum energy of 2 MeV. The crystals were mounted on a three-axis goniometer head allowing a resettability better than 0.05°. The beam current was limited to 10 nA on a spot size area of about 1 mm². The detection of the backscattered particles was made by a 13-keV resolution implanted junction set at 150° toward and off the beam axis. In order to restrict any additional damage due to the analyzing beam itself, the alignment procedure was performed on a virgin part of the crystal. Then the channeling spectrum was recorded after translating the sample holder so that the $^4\text{He}^+$ particles collide the uranium-irradiated zone. Moreover, some RBS-C experiments were carried out, on the same sample, using different $^4\text{He}^+$ energies (0.6, 1, 1.5, and 2 MeV). In this way, by studying the energy dependence of the dechanneling cross section, one can obtain complementary informations about the type of defects present in irradiated sapphire.

Optical absorption data were obtained at 300 K using a Cary 2300 spectrophotometer in the 185–1500 nm wavelength range. In these experiments, the incident light crossed the samples parallel to the direction of the uranium ion beam. As a consequence, whatever their depth location, all the absorption centers induced by the irradiation will contribute to the resulting optical density. The amount $N_F$ of oxygen vacancies per centimeter square was determined by using Smakula's formulas[43] given by

$$N_F = 2.05 \times 10^{17} \frac{n}{f(n^2+2)^2} \text{OD} W_{1/2} , \qquad (1)$$

where $f = 0.92$ is the oscillator strength of the optical transition (taken from Ref. 44), and $n = 1.8$ the refractive index of sapphire at the wavelength corresponding to the absorption band peak for $F$ centers (taken from Ref. 45). The term $W_{1/2}$ represents the half width (in eV) at half maximum of the optical absorption band characterized by a maximum optical density (OD).

### III. RESULTS AND DISCUSSION

#### A. RBS-C analysis

Figure 1 shows typical backscattering spectra obtained from a 2-MeV $^4\text{He}^+$ analysis of irradiated samples at an energy of 2.78 MeV/u. Spectra $(a)$, $(b)$, and $(c)$, recorded in channeling geometry, correspond to the three fluences used (up to $2.5 \times 10^{12}$ ions cm$^{-2}$). The aligned and random spectra [curves $(d)$ and $(e)$, respectively] obtained on a virgin crystal are also presented for comparison.

Before irradiation, a minimum yield $\chi_V = 2.7\%$ was measured at the low-energy side of the Al surface peak. This low value, typical in a single alignment geometry, gives evidence of the high-crystalline quality of the $\text{Al}_2\text{O}_3$ wafers after the preannealing at 1723 K for 120 h. After irradiation, a general increase of the backscattering yield with fluence is observed in channeling conditions. This indicates a defect creation process in both oxygen and aluminium sublattices. The sensitivity of $\alpha$-$\text{Al}_2\text{O}_3$ to such
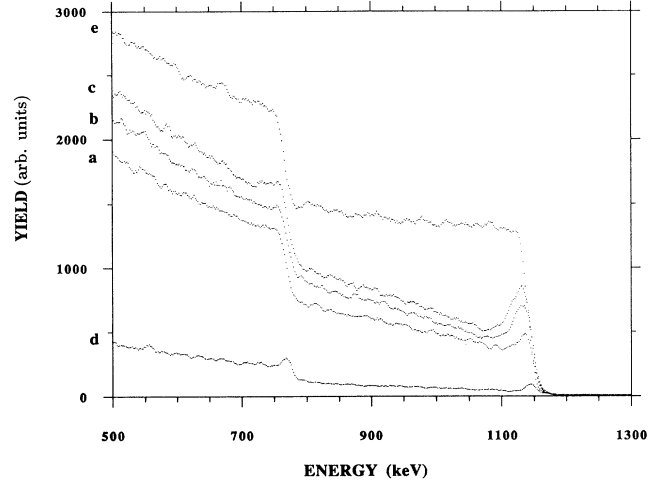


FIG. 1. RBS spectra for $\alpha$-$\text{Al}_2\text{O}_3$ irradiated with $^{238}\text{U}$ ions of 662-MeV incident energy. $(a)$ $1.2 \times 10^{12}$ ions cm$^{-2}$ (aligned), $(b)$ $2.1 \times 10^{12}$ ions cm$^{-2}$ (aligned), $(c)$ $2.46 \times 10^{12}$ ions cm$^{-2}$ (aligned), $(d)$ virgin sample (random), and $(e)$ virgin sample (aligned). Analysis conditions: 2-MeV $^4\text{He}^+$ ions; detection angle $= 150°$.

irradiations characterized by very high electronic stopping powers, previously reported by Canut *et al.*,[36] is hence confirmed. Due to the overlapping of oxygen and aluminium spectra and to the lack in RBS sensitivity for detecting low atomic masses, the disorder calculations have been carried out only from the aluminium signal. The dechanneling yield $\chi_0$ of the irradiated sample was measured behind the Al surface peak. By taking into account the minimum yield $\chi_v$ corresponding to the pristine crystal, the relative disorder $\alpha$ near the sample surface will be given by the classical formulas[46]

$$\alpha = \frac{\chi_0 - \chi_v}{1 - \chi_v} . \qquad (2)$$

Such a procedure requires some comments.

(i) The disorder calculations do not take into account the Al surface peak. This latter is clearly visible at the high-energy edge of RBS-C spectra, especially for the highest fluences. It indicates an excess of displaced aluminium atoms from the surface to a few tens of nanometers.

(ii) Even for the highest degrador thickness (30 $\mu$m Al), the range of the incident $^{238}\text{U}$ ions exceeds the maximum depth probed by the 2-MeV $^4\text{He}^+$ analysis beam (4.5 $\mu$m). Consequently, except the above-mentioned increase of disorder at the surface, no deep evolution of $\alpha$ can be extracted from RBS data. In particular, the nuclear damage peak, located around the projected range $R_p$ (see the values in Table I), cannot be evidenced by these channeling experiments.

Figure 2 represents, for the four incident used energies, the evolution of $\alpha$ versus the fluence $\Phi$. Assuming the absence of any annealing, a direct impact model[47] for defect creation predicts a kinetics which is given by
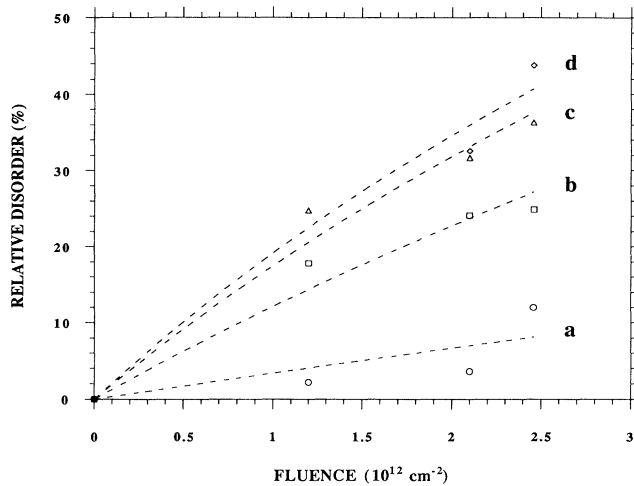
FIG. 2. Fluence and energy dependence of the damage in irradiated sapphire: (a) 115 MeV, (b) 410 MeV, (c) 662 MeV, and (d) 809 MeV.



FIG. 3. Evolution of the damage cross section vs the electronic stopping power.

$$\alpha = 1 - \exp(-A_e\Phi) \, , \qquad (3)$$

where $A_e$ is the damage cross section. Satisfactory fittings of the experimental data were obtained by using this expression (dashed lines in Fig. 2). The resulting damage cross sections $A_e$ are listed in Table II. The theoretical damage cross sections $A_n$, corresponding to target atoms elastically displaced, are also presented for comparison. The $A_n$ values have been calculated by dividing the displacement yields $Y_n$ (see Table I) by the molecular concentration of sapphire ($2.35 \times 10^{22}$ $Al_2O_3$ cm$^{-3}$). Whatever the irradiation conditions used in this work, it is evident that the nuclear contribution $A_n$ for defect creation in the first $\mu$m is negligible in respect with the measured value $A_e$. On the other hand, $A_n$ varies conversely with $(dE/dx)_e$. As presented in Fig. 3, this trend is at the opposite of the $(dE/dx)_e$ dependence of $A_e$. So, the disorder measured by RBS-C experiments

TABLE II. Comparison between the experimental damage cross section $A_e$, corresponding to a defect radius $r = (A_e/\pi)^{1/2}$, and the nuclear damage cross sections $A_n$ deduced from $Y_n$. $L$ is the track length, estimated from the measured electronic stopping power threshold (see text). In the last column, $N_n$ is the number of target atoms elastically displaced per one incident ion.

| $\left[\dfrac{dE}{dx}\right]_e$ (keV nm$^{-1}$) | $A_e$ (cm$^2$) | $r$ (nm) | $A_n$ (cm$^2$) | $\dfrac{A_e}{A_n}$ | $L$ ($\mu$m) | $N_n$ |
|---|---|---|---|---|---|---|
| 44.2 | $2.1 \times 10^{-13}$ | 2.59 | $2.5 \times 10^{-16}$ | 840 | 19.6 | 91 900 |
| 42.7 | $1.9 \times 10^{-13}$ | 2.46 | $3.2 \times 10^{-16}$ | 590 | 16.2 | 89 900 |
| 38.8 | $1.3 \times 10^{-13}$ | 2.03 | $4.3 \times 10^{-16}$ | 300 | 10.1 | 85 000 |
| 24.0 | $3.2 \times 10^{-14}$ | 1.01 | $1.2 \times 10^{-15}$ | 30 | 1.2 | 71 200 |

has to be attributed to collective electronic excitations. The mean radius $r$ of the damaged zones has been calculated from $A_e = \pi r^2$ and varies between 1.1 and 2.6 nm (see Table II). A linear regression (solid line) of the experimental points displayed in Fig. 3 intercepts the horizontal axis at about 21 keV nm$^{-1}$. This value may be regarded as the electronic stopping power threshold for defect creation in $\alpha$-$Al_2O_3$. This result explains why Sigrist and Balzer[26] did not evidence any latent track revelation in sapphire irradiated by fission fragments. As a matter of fact, the electronic stopping power used in this pioneering work never exceeded 15 keV nm$^{-1}$ in $\alpha$-$Al_2O_3$ (irradiations with [127]I ions of 40-MeV incident energy).

These results exhibit a good correlation between the damage cross section and the electronic stopping power, as shown in Fig. 3. However, the velocity of the incident ions may also play a role in the defect creation. Recent measurements in magnetic insulators[48,49] and lithium niobate[50] showed that at one given value of $(dE/dx)_e$ the damage cross section is higher at low ion velocity than at high velocity over a large range of $(dE/dx)_e$. This mechanism is related to the radial spreading of the deposited energy, which increases conversely with the ion velocity, according to the theoretical calculations of Katz[51] and Waligorski.[52] In a previous work,[41] using [208]Pb ion irradiations at 77 K, a damage cross section of $10^{-13}$ cm$^2$ was measured. The incident energy and the electronic stopping power were, respectively, 3.5 MeV/u and 40 keV nm$^{-1}$. In the present work, the damage cross section increases to $1.5 \times 10^{-13}$ cm$^2$ (see Fig. 3) for the same electronic stopping power. This difference can be explained by the lower velocity of uranium ions ($\beta = 6.1\%$) comparing to the velocity of lead ions ($\beta = 8.7\%$).

As pointed out in the experimental procedure, it is possible to evidence the major type of defects present in the crystal by varying the incident energy of the [4]He$^+$ beam used in RBS-C analysis. Let us consider the aligned spectra displayed in Fig. 1: on the low-energy side of the aluminium surface peak, the dechanneling yield $\chi$ in-

creases conversely with the energy. This phenomenon is due to the progressive misalignment of the analyzing beam after passing through a damaged layer of increasing thickness. Assuming the dechanneling events to obey the single scattering approximation[53] and provided that the disorder distributions are identical in the aluminium and oxygen sublattices, the evolution of $\chi$ versus depth $t$ may be deduced from the following equation:[54]

$$\frac{1-\chi(t)}{1-\chi_v(t)}$$
$$=[1-\alpha(t)]\exp\left[-(\sigma_{dAl}N_{Al}+\sigma_{dO}N_O)\int_0^t\alpha(u)du\right],$$
(4)

where $\alpha(t)$ is the relative disorder at a depth $t$ beneath the surface. $N_{Al}=4.7\times10^{22}$ cm$^{-3}$ and $N_O=7.05\times10^{22}$ cm$^{-3}$ are the atomic concentrations of the target species. $\sigma_{dAl}$ and $\sigma_{dO}$ are the dechanneling cross sections of aluminium and oxygen atoms, respectively.

As previously discussed, in the present work, $\alpha$ may be regarded as constant over the energy range covered by the aluminium RBS signal. In addition, we shall neglect the small increase of $\chi_v$ versus $t$. So, by taking into account Eq. (2), Eq. (4) may be simplified as

$$\chi(t)=1-(1-\chi_0)\exp[-(\sigma_{dAl}N_{Al}+\sigma_{dO}N_O)\alpha t],$$
(5)

which leads to the following expression for the initial slope of the dechanneling yield versus depth curve:

$$\left[\frac{d\chi}{dt}\right]_{t=0}=(1-\chi_0)(\sigma_{dAl}N_{Al}+\sigma_{dO}N_O)\alpha.$$
(6)

It may be rewritten as

$$\left[\frac{d\chi}{dt}\right]_{t=0}=(1-\chi_0)\sigma_d N_{Al}\alpha,$$
(7)

where $\sigma_d$ is a "global" dechanneling cross section given by

$$\sigma_d=\sigma_{dAl}+\tfrac{3}{2}\sigma_{dO}.$$
(8)

Equation (7) allows the determination of $\sigma_d$ at given analysis conditions, assuming convenient energy-depth calibration of the RBS-C signal. The procedure described above to calculate $\sigma_d$ neglects the influence of the aluminium surface peak onto the dechanneling process. In order to restrict the uncertainties resulting from such an approximation, the $\sigma_d$ calculations have been performed only for the lowest fluence (1.2$\times$10$^{12}$ cm$^{-2}$) which corresponds to the least excess of damage at the surface. Although the dechanneling cross sections of each atomic species cannot be extracted from (7) and (8), it seems reasonable to assume the same energy dependence for both $\sigma_{dAl}$ and $\sigma_{dO}$. As a consequence the evolution of $\sigma_d$ versus the analysis beam energy $E$ will give qualitative information about the main type of defects present in the first micrometers of the irradiated samples. Three major trends may occur: (i) For dislocation loops, $\sigma_d$ varies as $E^{1/2}$ at low energies.[55] At high energies
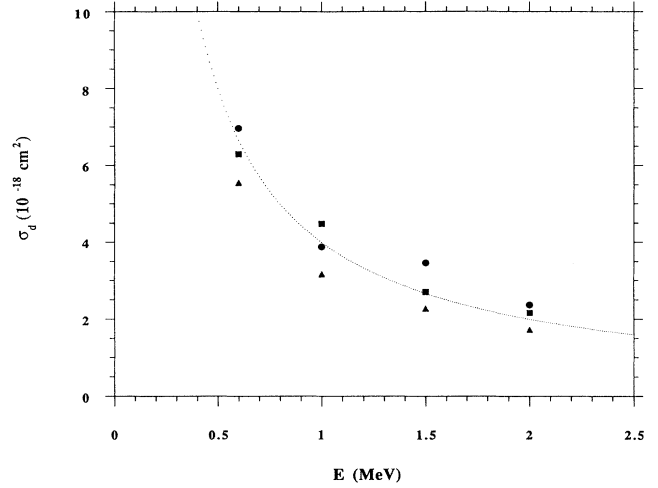


FIG. 4. Dechanneling cross section $\sigma_d$ of irradiated $\alpha$-Al$_2$O$_3$ vs the energy of the beam used for RBS-C analysis. Irradiation energies: 115 MeV (dots), 410 MeV (triangles), and 662 MeV (squares). The dashed line represents the best fit of the experimental data, using a $(1/E)$ dependence of $\sigma_d$.

(typically above $\approx 3$ MeV for $^4$He$^+$ particles), $\sigma_d$ becomes independent of $E$ for this type of defect.[56] (ii) For stacking faults and large size (mean diameter $> 100$ nm) voids, $\sigma_d$ is independent of $E$.[57] (iii) For displaced atoms and amorphized regions, $\sigma_d$ varies as $1/E$.[58]

Figure 4 represents the energy dependence of the dechanneling cross section deduced from RBS-C experiments on sapphire irradiated with $^{238}$U ions at the same fluence of $1.2\times10^{12}$ ions cm$^{-2}$. The $\sigma_d$ measurements were performed for each incident energy of the uranium ions. As the plot shows, the data are fitted by a $1/E$ law to a good degree of approximation. This result indicates that the disorder in irradiated $\alpha$-Al$_2$O$_3$ consists mainly of displaced atoms or amorphous regions, according to (iii). In addition, Fig. 4 does not exhibit any significant difference between the four $\sigma_d$ values at a given analysis energy. This leads to the conclusion that, whatever the uranium energy used in this work, the damage morphology in the first micrometers remains roughly the same.

## B. Optical absorption analysis

The optical absorption of the irradiated samples was investigated as a function of both ion fluence and electronic stopping power. A typical spectrum, corresponding to an irradiation fluence of 2.5$\times$10$^{12}$ ions cm$^{-2}$ at an incident energy of 115 MeV, is displayed in Fig. 5. As can be seen, Fig. 5 exhibits a major absorption band around 6.05 eV associated with two weaker side bands located at 5.4 and 4.8 eV. These three bands are related to oxygen vacancies which may contain either two electrons ($F$ center) or one electron ($F^+$ center). These defects induce an optical absorption in the near ultraviolet at 6.05 eV (corresponding to a wavelength of 206 nm) for the $F$ band or 4.8 eV (258 nm) and 5.4 eV (230 nm) for the $F^+$ band. Moreover, according to Dalal *et al.*,[59] another
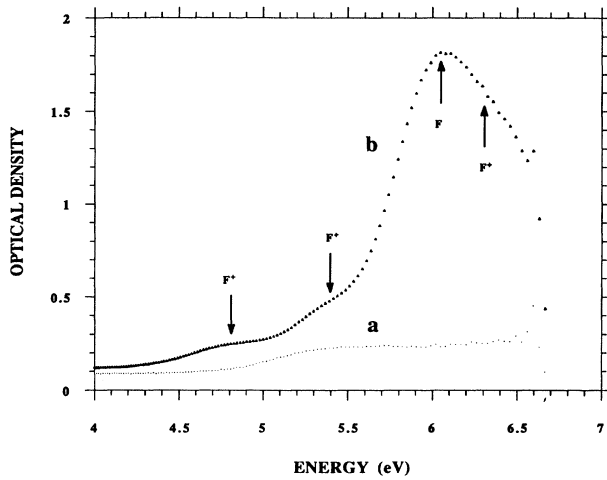
FIG. 5. Typical absorption spectra recorded on $\alpha$-Al$_2$O$_3$ before (a) and after (b) irradiation with $^{238}$U ions of 115-MeV incident energy (fluence: $2.46 \times 10^{12}$ ions cm$^{-2}$). The arrows indicate the positions of the characteristics $F$ and $F^+$ bands.

band located at 6.3 eV could also be ascribed to the $F^+$ center. This latter band is not clearly visible on Fig. 5. However, its presence could explain the asymmetry of the main peak located at 6.05 eV. Figure 6 represents for three $(dE/dx)_e$ values, the kinetics of the oxygen vacancy creation $N_F$. The data points have been calculated by applying Eq. (1) to the major absorption peak located at 6.05 eV. In this procedure, the raw spectral data have been corrected by a baseline substraction and the small contributions of the $F^+$ bands have been eliminated by interpolation. The kinetics exhibit the same shape: a rapid increase of $N_F$ at low fluences, followed by the beginning of a saturation effect for the highest $\Phi$ values. Few differences exist between the kinetics relative to the highest electronic stopping powers (42.7 and 38.8
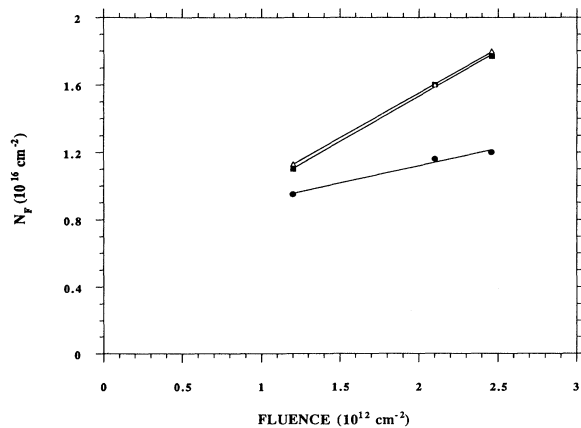


FIG. 6. Fluence evolution of the amount $N_F$ of $F$ centers, for three incident electronic stopping powers: 24 keV/nm (dots), 38.8 keV/nm (squares), and 4.27 keV/nm (triangles). The solid lines are drawn to guide the eye.

keV nm$^{-1}$). However, a significant decrease of the saturation level is evidenced in the third plot $[(dE/dx)_e = 24$ keV nm$^{-1}]$. Differently from RBS-C analysis which allows one to evidence lattice disorder only in the near subsurface, the absorption spectroscopy "integrates" all the point defects present in the irradiated sample. However, it is possible to precisely determine the depth location of the observed $F$ centers by studying the consequences of two hypotheses (a) and (b) presented below.

(a) Presence of $F$ centers in the $(dE/dx)_e$ damaged zone? This first hypothesis follows a description, proposed by Dartyge et al.,[60] which assume the coexistence of both point and extended defects along the ion track. According to these considerations, it seems reasonable to link the amount $N_F$ of oxygen vacancies with the amount $Q_e$ of displaced atoms by electronic processes. Given, as a first-order approximation,

$$N_F = \lambda Q_e , \tag{9}$$

where $\lambda$ is a constant.

In order to express $Q_e$, we assume that the damage induced by electronic processes extends to a maximum depth $L$. As a first-order approximation, the relative disorder will decrease linearly from $\alpha$ at the sample surface (RBS-C measurements) to zero at this maximum depth $L$. This leads to the following equation:

$$Q_e = N_{Al_2O_3} \int_0^L \alpha \left[ 1 - \frac{x}{L} \right] dx , \tag{10}$$

where $N_{Al_2O_3}$ is the atomic density of alumina $(2.35 \times 10^{22}$ Al$_2$O$_3$ cm$^{-3})$.

The integration of (10) gives

$$Q_e = \alpha N_{Al_2O_3} \frac{L}{2} . \tag{11}$$

At a given incident energy, the damaged depth $L$ may be estimated from the $(dE/dx)_e$ threshold (21 keV nm$^{-1}$) previously mentioned. According to the TRIM91 code, the energy and projected range corresponding to an electronic stopping power of 21 keV nm$^{-1}$ are $E_0 = 89$ MeV and $R_{p0} = 6.6$ $\mu$m, respectively. In other words, the last 6.6 micrometers of the ion range are practically free of $(dE/dx)_e$-induced damage. As a consequence, the damaged depth $L$ will be simply given by

$$L = R_p - R_{p0} . \tag{12}$$

The numerical values of $L$ are listed in Table II. By taking into account (9) and (11), one obtains

$$\frac{2N_F}{\alpha N_{Al_2O_3}} = \lambda L . \tag{13}$$

This equation supplies a criterion for testing hypothesis (a). As a matter of fact, by introducing a variable $y = 2N_F / \alpha N_{Al_2O_3}$, the curve $y = f(L)$ should exhibit a positive slope. For every irradiation condition, $y$ has been calculated from RBS-C and optical results and plotted versus $L$ [calculated from (12)] in Fig. 7. Despite an important scatter of the data observed at a given $L$ value,
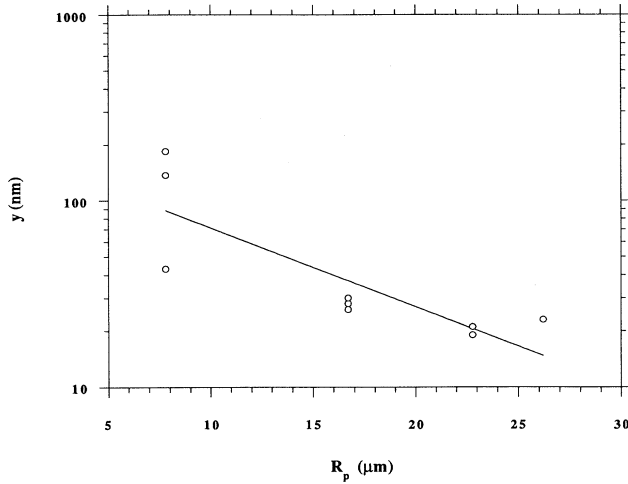
B. CANUT *et al.*



FIG. 7. Test of the presence of $F$ centers in the $(dE/dx)_e$ damaged zone. The decrease of the variable $y = 2N_F/\alpha N_{Al_2O_3}$ vs the track length $L$ is in conflict with this hypothesis.
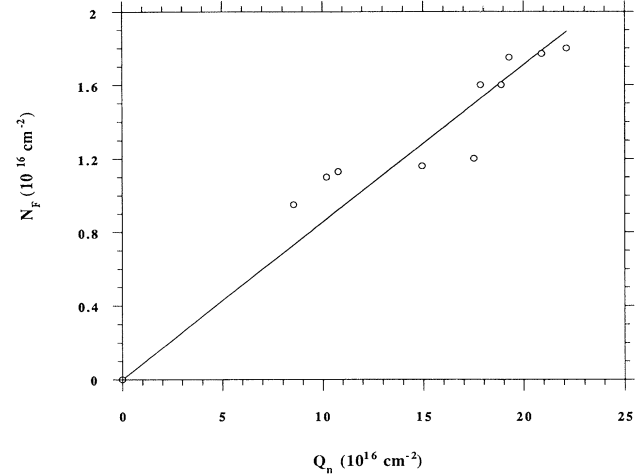
FIG. 8. Test of the presence of $F$ centers in the $(dE/dx)_n$ damaged zone. The strong correlation between $N_F$ and the amount $Q_n$ of displaced $Al_2O_3$ (calculated from the TRIM91 code), at a given fluence, supports this hypothesis.

Fig. 7 evidences a decrease of $y$ versus $L$. This trend is at the opposite to the expected one. As a conclusion, the $F$ centers present in sapphire after irradiation are probably not located in the $(dE/dx)_e$ damaged zone.

(b) Presence of $F$ centers in the predominantly $(dE/dx)_n$ damaged zone? According to this second hypothesis, a strong correlation should exist between $N_F$ and the amount $Q_n$ of displaced atoms by nuclear processes. This latter parameter can be easily calculated, at a given fluence $\Phi$, by using the following relation:

$$Q_n = N_n \Phi , \qquad (14)$$

where $N_n$ is the number of atomic species elastically displaced by each incident ion. The numerical values of $N_n$, calculated by using TRIM91 code, are listed as a function of the incident energy in Table II. As evidenced in Fig. 8, the expected correlation between $N_F$ and $Q_n$ occurs. One can thus conclude that the major part of the $F$ centers present in irradiated sapphire are created by nuclear processes, at the end of the ion range. It has to be noticed that the slope of the regression straight line is quite below the unity. This feature can be explained by recombination processes.

## IV. CONCLUSION

This work confirms that high-energy heavy-ion irradiations induce both point and extended defects in $\alpha$-$Al_2O_3$.

The lattice disorder evidenced by RBS-C analysis performed on samples bombarded with $^{238}U$ ions in the GeV range has been attributed to collective electronic excitations. The corresponding damage cross section $A_e$ varies from 0.3 to $2.1 \times 10^{-13}$ cm$^2$ when the electronic stopping power $(dE/dx)_e$ increases from 24 to 44.2 keV nm$^{-1}$. The extrapolation of this dependence leads to a $(dE/dx)_e$ threshold for extended formation of about 21 keV nm$^{-1}$. By comparing these results with the ones previously obtained by means of $^{208}Pb$ ion irradiations, a velocity effect in damage creation is suspected. According to RBS-C analysis performed at different beam energies, the defects produced by cooperative electronic processes consist of displaced atoms. Complementary characterizations, like high-resolution electron microscopy or x-ray diffraction at glancing incidence, are required to complete the damage description. These techniques could also bring valuable information about the unexpected excess of disorder observed in the near subsurface of the irradiated samples. Optical absorption spectroscopy evidenced the characteristic bands associated with isolated defects. The oxygen vacancy amounts $N_F$ have been calculated for the different fluences $\Phi$ and $(dE/dx)_e$ used. The results indicate that the major part of these defects are created by elastic processes and are located in the predominantly $(dE/dx)_n$ damaged zone.

[1]G. W. Arnold, G. B. Krefft, and C. B. Normis, Appl. Phys. Lett. **25**, 540 (1974).

[2]K. H. Lee and J. H. Crawford, Jr., Phys. Rev. B **15**, 4065 (1977).

[3]J. H. Crawford, Jr., Nucl. Instrum. Methods B **1**, 159 (1984).

[4]N. Naramoto, C. W. White, J. M. Williams, C. J. McHargue, O. W. Holland, N. M. Abraham, and B. R. Appleton, J. Appl. Phys. **54**, 683 (1983).

[5]P. J. Burnett and T. F. Page, Radiat. Eff. **97**, 123 (1986).

[6]C. J. McHargue, in *Structure Property Relationships in Surface Modified Ceramics, NATO Advanced Study Institute,* edited by C. J. McHargue, R. Kossowsky, and W. O. Hofer (Kluwer, Dordrecht, 1989), p. 253.

[7]A. Turos, Hj. Matzke, and P. Rabette, Phys. Status Solidi A **64**, 565 (1981).

[8]L. Romana, P. Thevenard, B. Canut, G. Massouras, R. Brenier, and M. Brunel, Nucl. Instrum. Methods B **46**, 94 (1990).

[9]C. Donnet, G. Marest, N. Moncoffre, J. Tousset, A. Rahioui, C. Esnouf, and M. Brunel, Nucl. Instrum. Methods B **59/60**, 1205 (1991).

[10]T. Hoiki, A. Itoh, S. Noda, H. Doi, J. Kawamoto, and O. Kamigaito, Nucl. Instrum. Methods B **7/8**, 521 (1985).

[11]T. Hoiki, A. T. Hoiki, A. Itoh, S. Noda, H. Doi, J. Kawamoto, and O. Kamigaito, J. Mater. Sci. **21**, 1321 (1986).

[12]C. J. McHargue, Nucl. Instrum. Methods B **19/20**, 787 (1987).

[13]G. B. Krefft and E. P. Eernisse, J. Appl. Phys. **49**, 2725 (1978).

[14]S. M. M. Ramos, B. Canut, L. Gea, P. Thevenard, M. Bauer, Y. Maheo, Ph. Kapsa, and J. L. Loubet, J. Mater. Res. **7**, 178 (1992).

[15]N. Moncoffre, Nucl. Instrum. Methods B **59/60**, 1129 (1991).

[16]J. Davenas and P. Thevenard, Nucl. Instrum. Methods B **80/81**, 1021 (1993).

[17]G. H. Kinchin and R. S. Pease, Rep. Prog. Phys. **18**, 1 (1955).

[18]D. M. Parkin and C. A. Coulter, J. Nucl. Mater. **101**, 261 (1981).

[19]C. W. White, C. J. McHargue, P. S. Sklad, L. A. Boatner, and G. C. Farlow, Mater. Sci. Rep. **4**, 1 (1989).

[20]G. C. Farlow, C. W. White, C. J. McHargue, and B. R. Appleton, Proc. Mater. Res. Soc. Symp. **27**, 395 (1984).

[21]C. J. McHargue, P. S. Sklad, J. C. McCallum, C. W. White, A. Perez, E. Abonneau, and G. Marest, Nucl. Instrum. Methods B **46**, 74 (1990).

[22]C. W. White, G. C. Farlow, C. J. McHargue, P. Angelini, P. S. Sklad, M. B. Lewis, and B. R. Appleton, Nucl. Instrum. Methods B **7/8**, 473 (1985).

[23]B. Canut, L. Romana, P. Thevenard, and N. Moncoffre, Nucl. Instrum. Methods B **46**, 128 (1990).

[24]F. Clinard and L. W. Hobbs, in *Physics of Radiation Effects in Crystals,* edited by R. A. Johnson and A. N. Orlov (Elsevier, Amsterdam, 1986), Chap. 7.

[25]E. C. M. Silk and R. R. Barnes, Philos. Mag. **4**, 970 (1959).

[26]A. Sigrist and R. Balzer, Helv. Phys. Acta. **50**, 49 (1977).

[27]S. Klaumünzer and G. Schumacher, Phys. Rev. Lett. **51**, 1987 (1983).

[28]S. Klaumünzer, Ming-Dong Hou, and G. Schumacher, Phys. Rev. Lett. **57**, 850 (1986).

[29]A. Audouard, E. Balanzat, S. Bouffard, J. C. Jousset, D. Lesueur, and L. Thome, Europhys. Lett. **3**, 327 (1987); **5**, 241 (1988).

[30]S. Klaumünzer, Chang-Lin Li, S. Löffler, M. Rammensee, G. Schumacher, and H. C. Neitzert, Radiat. Eff. Def. Solids **108**, 131 (1989).

[31]A. Benyagoub, S. Löffler, M. Rammensee, S. Klaumünzer, and G. Saemann-Ischenko, Nucl. Instrum. Methods B **65**, 228 (1992).

[32]A. Benyagoub and S. Klaumünzer, Radiat. Eff. Def. Solids **126**, 105 (1993).

[33]R. L. Fleischer, P. B. Price, and R. M. Walker, *Nuclear Tracks in Solids* (California Press, Berkeley, 1975).

[34]A. Barbbu, A. Dunlop, D. Lesueur, and R. S. Averbach, Europhys. Lett. **15**, 37 (1991).

[35]A. Iwase, S. Sasaki, T. Iwata, and T. Nihira, Phys. Rev. Lett. **58**, 2450 (1987).

[36]A. Dunlop, D. Lesueur, G. Jaskierowicz, and J. Schildknecht, Nucl. Instrum. Methods B **36**, 412 (1989).

[37]F. Studer, C. Houpert, D. Groult, and M. Toulemonde, Radiat. Eff. Def. Solids **110**, 55 (1989).

[38]M. Toulemonde, G. Fuchs, N. Nguyen, F. Studer, and D. Groult, Phys. Rev. B **35**, 6560 (1987).

[39]F. Studer, D. Groult, N. Nguyen, and M. Toulemonde, Nucl. Instrum. Methods B **19/20**, 856 (1987).

[40]C. Houpert, N. Nguyen, F. Studer, D. Groult, and M. Toulemonde, Nucl. Instrum. Methods B **34**, 228 (1988).

[41]B. Canut, S. M. M. Ramos, P. Thevenard, N. Moncoffre, A. Benyagoub, G. Marest, A. Meftah, M. Toulemonde, and F. Studer, Nucl. Instrum. Methods B **80/81**, 1114 (1993).

[42]J. F. Ziegler, J. P. Biersack, and U. Littmark, *Stopping Power and Ranges of Ions in Matter* (Pergamon, New York, 1985), Vol. 1.

[43]A. Smakula, Z. F. Phys. **59**, 603 (1930).

[44]B. D. Evans and M. Staplebroek, Phys. Rev. B **18**, 7089 (1978).

[45]V. N. Abramov, B. G. Ivanov, and A. I. Kuznetsov, Phys. Status Solidi A **48**, 287 (1978).

[46]W. K. Chu, J. W. Mayer, and M. A. Nicolet, *Backscattering Spectrometry* (Academic, New York, 1978).

[47]J. F. Gibbons, Proc. IEEE **60**, 1062 (1972).

[48]F. Studer, C. Houpert, H. Pascard, R. Spohr, J. Vetter, J. Yun Fan, and M. Toulemonde, Radiat. Eff. Def. Solids **116**, 59 (1991).

[49]A. Meftah, F. Brisard, J. M. Costantini, M. Hage-Ali, J. P. Stoquert, F. Studer, and M. Toulemonde, Phys. Rev. B **48**, 920 (1993).

[50]B. Canut, R. Brenier, A. Meftah, P. Moretti, S. Ould Salem, S. M. M. Ramos, P. Thevenard, and M. Toulemonde, Nucl. Instrum. Methods B **91**, 312 (1994).

[51]R. Katz and E. J. Kobetich, Phys. Rev. **186**, 344 (1969).

[52]M. P. R. Waligorski, R. N. Hamm, and R. Katz, Nucl. Tracks Radiat. Meas. **11**, 309 (1986).

[53]E. Bogh, Can. J. Phys. **46**, 653 (1968).

[54]A. Benyagoub and L. Thome, Radiat. Eff. **105**, 9 (1987).

[55]Y. Quere, Phys. Status Solidi **30**, 713 (1968).

[56]H. Kudo, Phys. Rev. **18**, 5995 (1978).

[57]S. U. Campisano, C. Foti, E. Rimini, and S. T. Picraux, Nucl. Instrum. Methods **149**, 371 (1978).

[58]E. Rimini, S. U. Campisano, G. Foti, P. Baeri, and S. T. Picraux, *Ion Beam Surface Layer Analysis* (Plenum, New York, 1976).

[59]M. L. Dalal, M. Rahmani, and P. D. Townsend, Nucl. Instrum. Methods B **32**, 61 (1988).

[60]E. Dartyge, J. P. Duraud, Y. Langevin, and M. Maurette, Phys. Rev. B **23**, 5213 (1981).